Acoustic-induced velocity in a multi-orifice acoustic liner grazed by a turbulent boundary layer

Avallone, F.; Casalino, D.

Acoustic-induced velocity in a multi-orifice acoustic liner grazed by a turbulent boundary layer

F. Avallone* and D. Casalino [†]

Faculty of Aerospace Engineering, Delft University of Technology, Kluyverweg 1, 2629HS, Delft, The Netherlands

High-fidelity lattice-Boltzmann very-large-eddy simulations have been carried out to investigate the behaviour of a single-cavity multi-orifice acoustic liner grazed by a turbulent boundary layer at free-stream Mach number equal to 0.3 and an acoustic wave. Numerical results have been used to compute the acoustic-induced velocity within the liner orifice with a triple decomposition approach. It is shown that the acoustic-induced velocity presents a symmetric behaviour between the inflow and outflow cycles and that its amplitude is the same as for the case without turbulent grazing flow. The major differences when comparing the case with and without turbulent grazing flow is the spatial distribution within the orifice attributed to the presence of a quasi-steady vortex formed within the orifice visible from the time-averaged flow field. It is concluded that the increase of resistance in presence of a turbulent grazing flow is linked to a reduction of the effective orifice area as confirmed by the comparison between the mass-flow rates for the cases with and without grazing flow.

I. Introduction

The development of Ultra High Bypass Ratio (UHBR) engines, to reduce both fuel consumption and noise pollution, is challenging well-established noise reduction solutions, such as acoustic liners. UHBR are characterized by a larger fan diameter, a shorter nacelle, a lower rotational speed of the fan and a lower jet core velocity. As a consequence, the fan can become a dominant noise source also during take-off. The larger fan diameter represents a spatial constraint for the installation of acoustic liners. As a matter of fact, using current technologies, the thickness of the acoustic liner would naturally grow to accommodate the lower rotational velocity of the fan, thus increasing the overall drag. For this reason, future generations of acoustic liners need to be designed with innovative shapes such to be thinner that the actual ones. This engineering and scientific challenge need to be addressed quickly.

Even if the physics of the acoustic liners is well known when they are grazed only by acoustic waves and operate in the linear regime [1], there is still lack of understanding and modelling when they operate in real working conditions, i.e. they are grazed by a high-speed turbulent flow and high amplitude acoustic waves. As a matter of fact, under these conditions, the behaviour of these acoustic treatments is still poorly understood because of the complex flow field over the perforated plate and of the acoustic-flow interaction [2]. The lack of fundamental knowledge leads to a non-accurate modelling of the acoustic liners. In addition, a detailed description of the acoustic-flow interaction and its dependence on the orifice geometry can be used to design innovative solutions, which reduce acoustic noise with minimal drag penalties.

The analytical models, conventionally used for the design, assume that the interaction between the turbulent boundary layer, the acoustic waves and the perforated plate can be represented by an equivalent impedance, which shall not depend on the incident acoustic wave [3, 4]. This impedance condition, known as Ingard-Myers boundary condition [3, 5], has been studied with the goal of including all the relevant physical mechanisms [6–8]. Recent studies have pointed out the relevance of the wall shear stress at the interface of the acoustic treatment on the sound propagation [7, 8]. This effect was included in the modified Ingard-Myers boundary conditions as an additional coefficient that represents the transfer of momentum from the flow to the wall [6] or using a momentum transfer impedance [8]. However, these modifications are not able yet to explain some experimental contradictions, such as the dependence of the acoustic impedance on the relative direction between the convecting flow and the acoustic waves [8, 9]. It has been recently proven that this is caused by inaccurate modelling of the boundary conditions [10].

Despite the efforts made to describe this complex acoustic-flow interaction, these models still lack of an accurate physical description. This is due to the difficulties in measuring such small details (e.g., the vorticity field in the orifice and the shear stress on the perforated plate) under realistic conditions. For this reason, high-fidelity numerical

---

*Assistant Professor, AWEP Department, f.avallone@tudelft.nl, AIAA member
[†]Full Professor, AWEP Department, d.casalino@tudelft.nl, AIAA member

simulations, based on reference experiments carried out under realistic but controlled conditions, represent an interesting tool to detect and explain the most relevant flow features and gain insights on the fundamental physics.

A relevant contribution is the one by Zhang and Bodony [2] who performed Direct Numerical Simulation (DNS) of both a laminar and turbulent grazing flow with a normal incident acoustic wave. A relevant result of this work is the description of the complex acoustic-flow interaction at the interface, which confirms that the models do not include yet all the relevant physics. However, the adopted methodology, did not allow to replicate the realistic flow conditions from the reference experiments [11]; a simplification of the geometry (i.e., a single orifice) and a reduction of the cavity based Reynolds number were necessary. In addition to that, to reduce the computational cost, a time-varying boundary layer was simulated instead of a spatially varying one. To overcome this limitations, Sebastian *et al* [12] performed a Large Eddy Simulation (LES) of the flow in a duct where the wall was modelled with an impedance boundary conditions. The simulations highlighted the generation of instability waves, with wavelength larger than the turbulent flow structures, that modulate the turbulent structures and transport momentum toward the surface, thus affecting the flow-acoustic interaction; an effect that could not be visible in a non-spatially developing boundary layer.

However, in order to shed light on the relevant physical mechanisms, it is important to isolate the acoustic-induced velocity within the orifice at the face sheet from the velocity induced by the grazing turbulent flow. This study aims at filling this gap by describing the behaviour of the acoustic-induced velocity withing the orifice. To reach the goal, high-fidelity Lattice-Boltzmann Very-Large-Eddy-Simulations (LB/VLES) are carried out on a liner geometry previously tested both experimentally in the Grazing Flow Impedance Tube (GFIT) facility at NASA Langley Research Center and numerically by Zhang and Bodony [2]. Results from simulations with and without turbulent grazing flow at free-stream Mach number equal to 0.3 are compared.

The rest of the paper is structured as follows: the methodology is summarized in Section II while the computational setup is described in Section III. Acoustic impedance results and the velocity within the orifice are discussed in Section IV and V, respectively. A summary of the findings is reported in the conclusions.

II. Methodology

The commercial software 3DS Simulia PowerFLOW 6-2019 is used. The solver has been already validated for SDOF liner [13–16]. The same solver has been also used to simulate the effect of a SDOF liner installed on the nacelle of the NASA Source Diagnostic Test engine [17]; the predicted sound attenuation is in agreement with the one obtained with a different high-fidelity flow solver [18].

PowerFLOW is based on the LB method with collision relaxation time and distribution function dynamically calibrated to the time scales of slow turbulent structures, modelled through a turbulence transport model. The LB scheme is based on an expansion of the distribution function, solution of the Boltzmann equation, in a series of Hermite polynomials [19], which constitute an orthogonal basis particularly suited to describe a flow in the kinetic space. The expansion truncated at an order higher than 3 provides a unique representation of the macroscopic hydrodynamic status of a fluid. PowerFLOW uses a regularized collision operator in the non-dimensional LB equation, which includes terms proportional to the second order Hermite polynomials, accounting for energy and momentum fluxes, and third order terms polynomials, accounting for heat fluxes. Following Chen *et al* [20], a Galilean invariance is applied to the collision operator thus resulting in a two-term regularized form, in which the two terms account for energy/momentum fluxes and heat fluxes, respectively, with corresponding relaxation times related to the macroscopic fluid viscosity and thermal conductivity.

Another important component of the solver is turbulence modeling, which is key to tackle high Reynolds number flows. In PowerFLOW this is accounted by modifying the relaxation time in the collision operator by considering the time scales related to the turbulent motion and to the strain rate and rotation of the resolved flow field. Although the relaxation time is computed using a two-equation transport model, the k-ϵ Re-Normalization Group (RNG) model [21, 22], this is not used to compute an equivalent eddy viscosity, like in Reynolds-Averaged Navier Stokes models, but it is instead used to dynamically re-calibrate the Boltzmann model to the characteristic time scales of a turbulent flow motion. Hence, no Reynolds stresses are explicitly added to the governing equations, but they are an implicit consequence of the chaotic exchange of momentum driven by the turbulent flow with characteristic times smaller than the slowly-varying turbulent flow.

The LB/VLES equations are solved on a Cartesian mesh which is automatically generated for any complex shape of the boundary conditions. Variable Resolution (VR) regions can be defined in the flow domain to locally refine the grid size by successive factors of 2. By construction, in a time step particles are advected exactly from one point to the other points of the lattice stencils. Therefore, the local time step varies by a factor 2 in adjacent VRs. Bounce-back

2
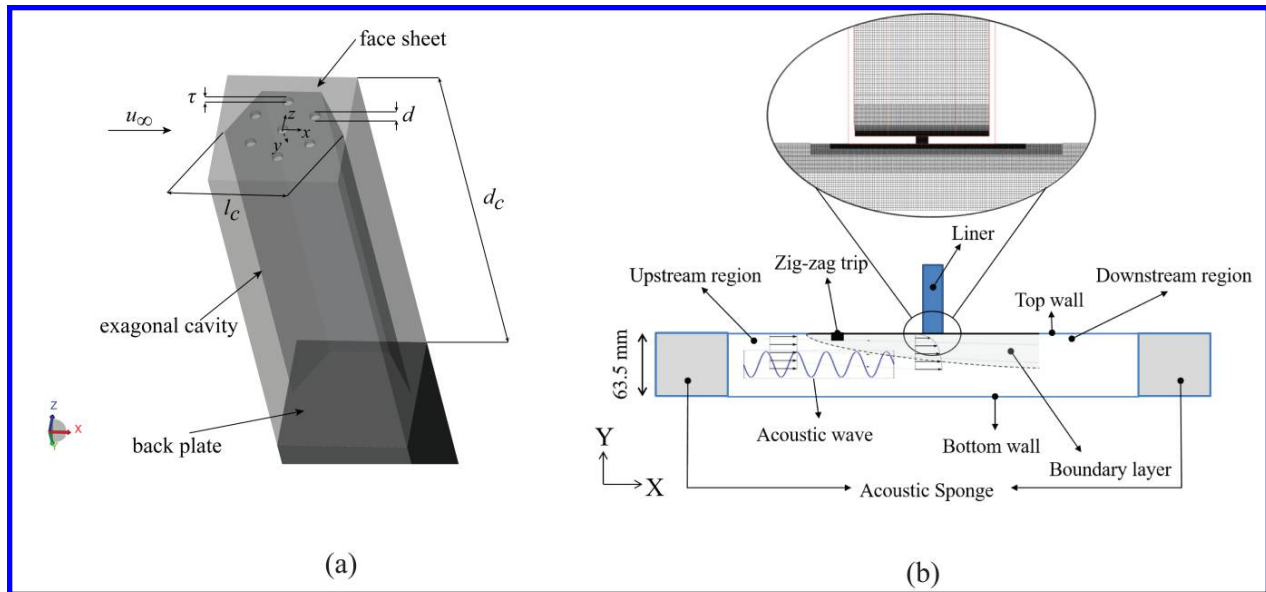
Fig. 1 (a) Schematic of the cavity with representation of the coordinate reference system. The y axis is oriented towards the inside of the cavity. (b) Schematic of the computational setup with the grid in a plane crossing the central orifice.

boundary condition for no-slip walls and the specular reflection for frictionless walls are ensured thanks to a generalized volumetric formulation for the intersection of arbitrary-oriented surface elements and the volume elements [**?**]. Finally, a wall model accounting for pressure gradients is used to boundary layer behaviours at high Reynolds numbers [22].

III. Computational setup

The acoustic liner geometry has been experimentally investigated by Jones *et al* [11] in the GFIT facility at NASA Langley Research Center at several free-stream Mach number and computationally investigated by Zhang and Bodony [2] at free-stream Mach number equal to 0.5. The liner is shown in Figure 1. A rigid face sheet of thickness $\tau = 0.64$ mm is perforated with cylindrical holes of diameter $d = 0.99$ mm, which corresponds to a length-to-diameter ratio of 0.65. A single honeycomb cavity with 7 orifices is studied, thus resulting in a porosity of $\sigma = 6.4\%$ very close to the reference study ($\sigma = 8.7\%$). While in the experimental study the orifices are randomly located such that they can overlap neighboring cavities, in this study, six orifices are placed at the center of each of the six equilateral triangles that form the hexagon and one at its center. The cell depth is $d_c = 38.10$ mm and the distance between the two opposite corners of the cell is $l_c = 9.5$ mm. A rigid back plate closes the cell from below and the cell walls are rigid, so that, in the experiments, neighboring cells cannot communicate.

The acoustic liner is grazed by a turbulent flow with free stream Mach number equal to $M_\infty = 0.3$. The liner is placed along the top wall of a duct that has a rectangular cross section with height equal to 63.5 mm, as in the GFIT facility, while the width is restricted to 12 mm to reduce the computational cost. Transition to turbulence is forced using a zig-zag strip at 1750 mm upstream of the liner. The zig-zag strip is 1 mm thick, it has length and wavelength equal to 10 mm and angle of 60°. The location of the zig-zag trip has been selected such to replicate the time-average turbulent boundary layer profile measured in the GFIT [23]. A schematic of the computational setup is reported in Figure 1, where an example of the computational grid close to cavity is shown. In the computations, 10 resolution regions are used; the smallest voxels are used to discretize the computational domain close and within the orifices. The maximum resolution adopted in this paper is 40 voxels/mm $\approx$ 40 voxels/d. This is similar to the value suggested by Manjunath *et al* [15] in absence of acoustic waves of $\approx$ 42 voxels/d.

Periodic boundary conditions are applied on the side walls, no-slip boundary condition on the top wall and slip boundary condition on the bottom wall. At the inlet, free stream velocity corresponding to the free-stream Mach number is assigned while pressure boundary condition is set at the outlet. Additional acoustic sponge regions, where viscosity is increased, are placed ad the inlet and outlet of the computational domain to dampen the reflection of acoustic waves.
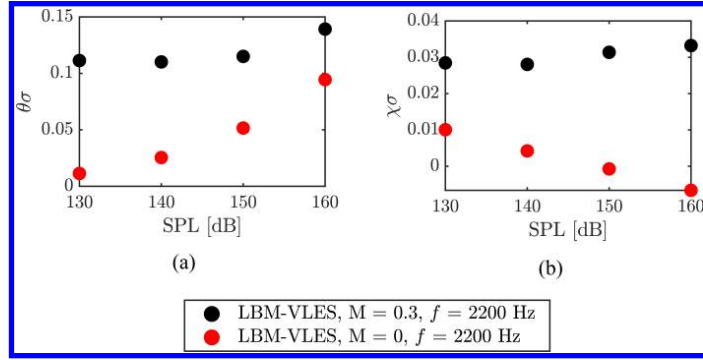
Fig. 2 **(left) Resistance θ and (right) reactance χ components of impedance scaled with the liner porosity σ. The frequency of the acoustic wave is 2200 Hz, while the amplitude varies between 130 and 160 dB.**

Computations are carried out with a two-step approach: first the turbulent boundary layer convecting in the duct is computed and temporal convergence is verified; an instantaneous flow field is saved and is modified by superimposing a plane acoustic wave, with given frequency and amplitude, using the *Opty∂B* toolkit. The modified flow field is used to seed the high-fidelity numerical simulations with acoustic wave. This approach has the advantage to reduce the computational cost when there is the need of studying many different configurations as in the present case.

Sixteen cases are investigated in order to cover a large range of conditions. The test matrix is summarized in Table 1 where the SPL has been calculated using reference pressure of 20×10^{-6} Pa. For all the investigated configurations, the acoustic wave propagates in the same direction as the mean flow.

Table 1   Test matrix

| SPL [dB]	f [Hz]	M
130,140,150,160	1800,2200,3000	0.3
130,140,150,160	2200	0

Surface data for the estimation of the impedance is sampled at a frequency of 20 kHz. The flow field is instead sampled such to have 720 point per wavelength. For each configurations, acoustic waves with 10 acoustic periods are considered based on the findings from previous studies from the authors [15, 16] and DNS results by Zhang and Bodony [2]. Data are sampled after convergence of the unsteady field, which is in general after no more than 2 acoustic periods.

IV. Acoustic impedance

The acoustic impedance, obtained with the method proposed by Dean [24], has been computed using the approach described by Manjunath *et al* [15]: time history of the surface pressure fluctuations on the face sheet are sampled every 30 degrees on a circumference of radius $1d$ from the center of each orifice, while, at the back plate, they are sampled in correspondence of the center of each orifice. Data are then averaged out of all the data points. The two components of the acoustic impedance, namely resistance θ and reactance χ, are plotted in Figure 2 scaled with the liner porosity σ. The figure compares the cases with (M=0) and without grazing turbulent flow (M=0.3) for varying SPL of the grazing acoustic wave and frequency equal to 2200 Hz. Only one frequency has been selected because negligible differences have been found in a previous study currently under review.

The figure shows that, increasing the SPL, θ increases more in absence of flow with respect to the case with grazing turbulent flow. As a matter of fact, while the former shows an exponential increase, the latter θ is almost constant up to 150 dB while, at higher SPL, it starts increasing. Furthermore, it is observed that, in presence of grazing flow, the amplitude of θ is almost comparable to the one for the largest SPL investigated at M=0. The presence of a grazing flow affects also the reactance χ; for M=0, χ decreases with the SPL while for M=0.3 it slightly increases with the SPL.

The values presented in Figure 2 are the average out of the 7 orifices. The comparison of the distribution of each of the components is reported in Figure 3 for the same conditions as above. In the figure, the error bar for each orifice represents the scatter between results obtained using each of the 30 data points around each orifice. It is shown that
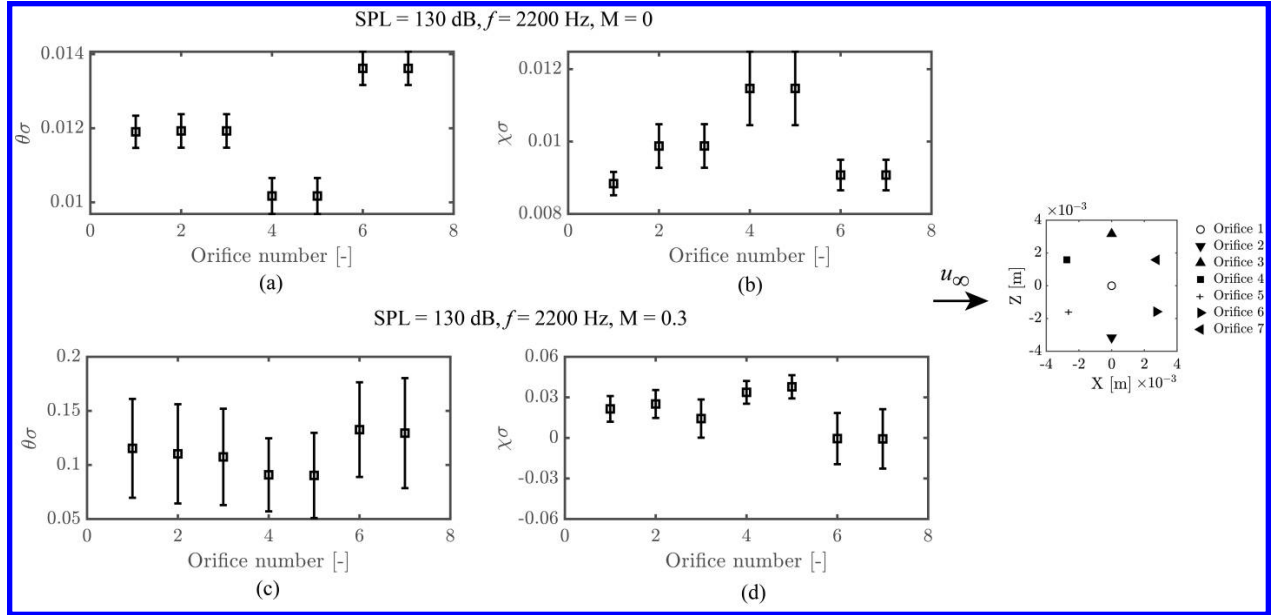
4

Fig. 3 (a-c) Reactance θ and (b-d) resistance χ components of impedance scaled with the liner porosity σ, for M = 0 (a-b) and M = 0.3 (c-d). The frequency of the acoustic wave is 2200 Hz, while the amplitude varies between 130 and 160 dB.

the presence of a turbulent grazing flow alters the amplitude of both components but not the distribution between the orifices. As a general consideration, it is possible to notice that the resistance tends to increase going from the most upstream to the most downstream orifices; this is attributed to the near wake of the most upstream orifice affecting the most downstream one. Conversely, the reactance decreases in the downstream direction. This finding confirms that the presence of turbulent flow enhances features which are however present also without flow.

V. Description of the flow within the orifice

Results discussed in the previous section have shown that the variation of acoustic impedance when a turbulent grazing flow is present affects the amplitude of both components of impedance but not their spatial distribution. Previous studies [2, 25] have shown that the flow in the orifice is strongly affected by the presence of the grazing turbulent flow but a clear link between the flow and the acoustic response of the liner has not been reported yet. In this section, the acoustic induced-velocity with and without grazing flow is linked to the acoustic impedance results discussed above.

Before describing the details of the flow within the orifice, an overview of the flow in absence of any acoustic wave is shown in Figure 4, where vortices are visualized using the λ_2 criterion. Zooms at the zig-zag trip location and in vicinity of the acoustic liner are also shown. The figure shows that the zig-zag trip is forcing transition and that a turbulent boundary layer develops downstream; the spatially developing turbulent boundary layer convects over the liner; at the face sheet, the flow interacts with the orifices, injecting vorticity within the cavity. These observations confirm the presence of a recirculation within the orifice, that might affect the interaction between the grazing acoustic wave and the liner.

In order to separate the effects of the mean flow from the one induced by the grazing acoustic wave, a triple decomposition of the velocity components is performed. The time-series obtained from the LB/VLES simulations are first phase locked with the incoming acoustic wave; the phase-locked velocity components are indicated as $\tilde{u},\tilde{v},\tilde{w}$. Phase-locked results are then averaged and the resulting velocity components are indicated as $\bar{u},\bar{v},\bar{w}$. Finally, the acoustic-induced velocity is obtained by subtracting the phase-averaged field from the phase-locked fields and the three velocity components are indicated as $\bar{\bar{u}},\bar{\bar{v}},\bar{\bar{w}}$. In the rest of the paper, the shear velocity upstream of the liner in absence of acoustic wave is used as reference scale velocity (u_τ) [25]. Furthermore, in the following, $\phi = 0$ is defined as the phase when the acoustic pressure reaches the maximum at the center of the liner outside of the turbulent boundary layer.

As shown above, the turbulent boundary layer grazing over the liner causes local flow recirculation within the orifice. This is better shown by the streamlines of the time-averaged flow superimposed to the contour plot of $\bar{v}$ in Figure 5. The
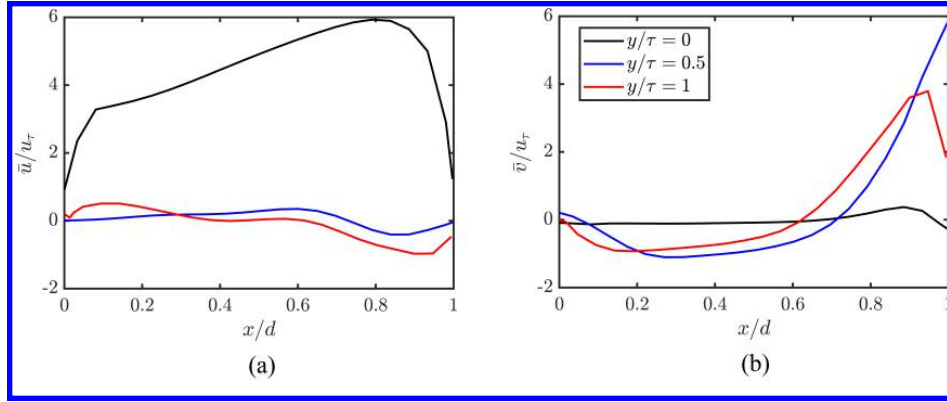
5
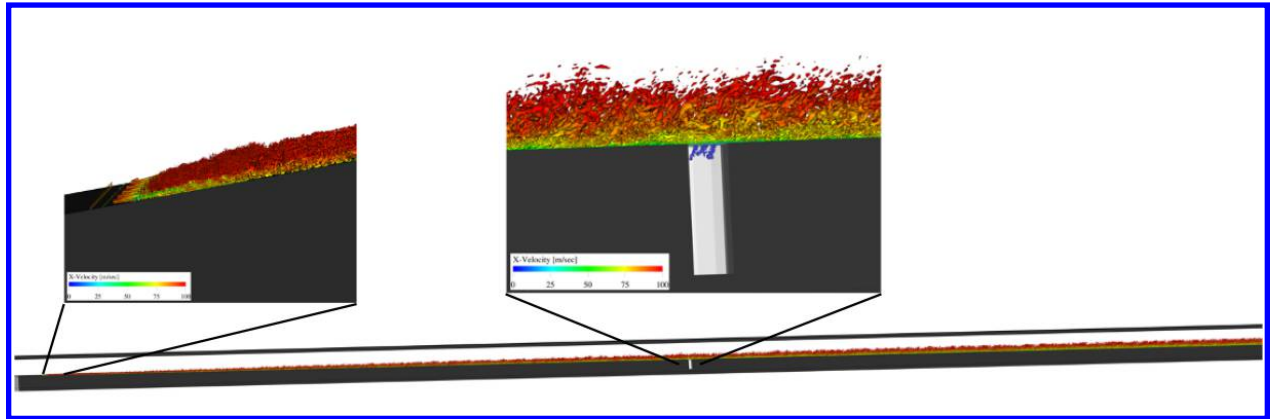
Fig. 4 Instantaneous flow field with zoom at the zig-zag location and at the acoustic liner location. Vortices are visualized using the λ_2-criterion.
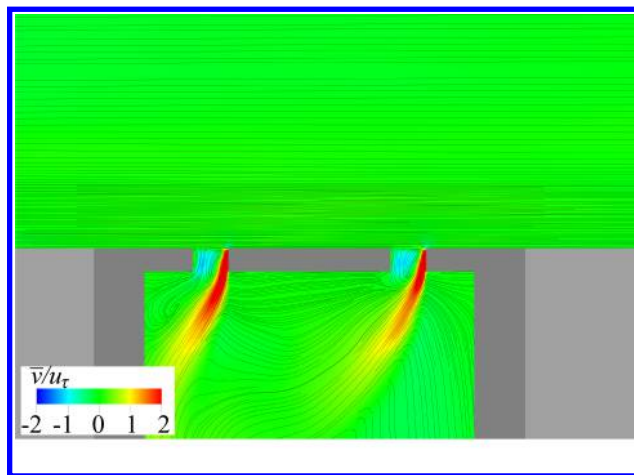
Fig. 5 Time-averaged flow field: vertical velocity component $\bar{v}$ with streamlines.

Fig. 6 Time-averaged velocity components: (a) streamwise $\bar{u}$ and (b) wall-normal $\bar{v}$.

vortex core is located at the downstream half of the orifice and results in a positive $\bar{v}$ at the downstream edge of the orifice and negative $\bar{v}$ at the upstream edge. In the rest of the paper, this vortex is defined as quasi-steady because flow visualizations have shown that it slightly oscillates within the orifice.

To better quantify the velocity induced in the orifice by the quasi-steady vortex, the distributions, along the diameter of the upstream orifice, of both $\bar{u}$ and $\bar{v}$ at y/τ equal to 0, 0.5, 1 are shown in Figure 6. At y/τ equal to 0 (i.e. over the face sheet), $\bar{u}/u_\tau$ increases from the upstream to the downstream edge from 4 to 6; towards the downstream edge ($x/d > 0.6$), the flow is oriented towards the inside of the cavity.

Before showing the acoustic-induced vertical velocity component, the phase-locked vertical velocity component $\tilde{v}$ within the orifice at the same wall-normal locations as above, for the case with grazing turbulent boundary layer, is plotted in Figure 7. Each column of the figure shows a different SPL of the grazing acoustic wave.

At $y/\tau = 0$ (Figure 7a), increasing the SPL, the location of the maximum $\tilde{v}$ moves from the downstream edge towards the center of the cavity, while the location of the minimum of $\tilde{v}$ is always located at the downstream edge of the orifice at approximately $x/d = 0.8$. At y/τ equal to 0.5 and 1, the flow accelerates within the orifice and the maximum of $\tilde{v}$ is located at the downstream edge. For phase angles $\phi > 180°$, the spatial distribution along the diameter flattens and it resembles more the one expected in absence of flow [2, 15]. This result is in agreement with the findings of Zhang and Bodony [2], and Léon *et al* [25], who showed an asymmetry between the inflow and outflow cycles of the same liner geometry under grazing flow. This asymmetry led to the definition of two distinct discharge coefficients for the outflow and inflow phases.

Figure 7 also shows that, independently on the SPL, the maximum $\tilde{v}$ is larger than the minimum one and the former reaches always a peak at x/d approximately equal to 0.8. However, the results from the mean flow (Figure 5) have shown that phase-locked results might be affected by the presence of the quasi-steady vortex formed within the orifice. For this reason, the acoustic-induced velocity has been computed and shown in Figure 8; since the vertical velocity component $\bar{\bar{v}}$ is the one associated to the conversion of acoustic energy in kinetic energy, this is the only one plotted.

When removing the mean flow from the phase-locked velocity field, the inflow and outflow cycles show a symmetric behaviour. At $y/\tau = 0$, it is found that the distribution of $\bar{\bar{v}}$ is almost symmetrical with respect to $x/d = 0.5$, thus suggesting that the acoustic liner behaves similarly to the no-flow case (as also shown by the impedance component in Figure 2). Within the orifice (y/τ equal to 0.5 and 1), there is always spatial asymmetry with respect to the orifice center with the maximum and minimum of $\bar{\bar{v}}$ located at the downstream half of the orifice at approximately $x/d = 0.8$. Increasing the SPL, the maximum of $\bar{\bar{v}}$ spreads over a wider x/d range.

For all the cases, it is evident that only the downstream half of the orifice shows a periodic variation of the acoustic-induced velocity. At the centerline of the orifice, the streamwise extension of this region grows with increasing the SPL. The x/d range where a periodic variation of $\bar{\bar{v}}$ is observed corresponds to the x/d range with a positive $\bar{v}$ (Figure 6b), thus suggesting that the quasi-steady vortex formed within the orifice affects the liner behaviour. It is also observed that the time-averaged streamwise velocity component has also a relevant effect on the amplitude and spatial distribution of $\bar{\bar{v}}$ within the orifice. When the acoustic-induced velocity is larger than $\bar{u}$, then the quasi-steady vortex within the orifice does not act as a barrier to the acoustic wave.

Figure 9 compares the acoustic-induced velocity for the flow (continuous line) and no-grazing flow (dashed lines) cases . The figures clearly show that $\bar{\bar{v}}$ reaches the same maximum value for both cases. The minor differences shown in
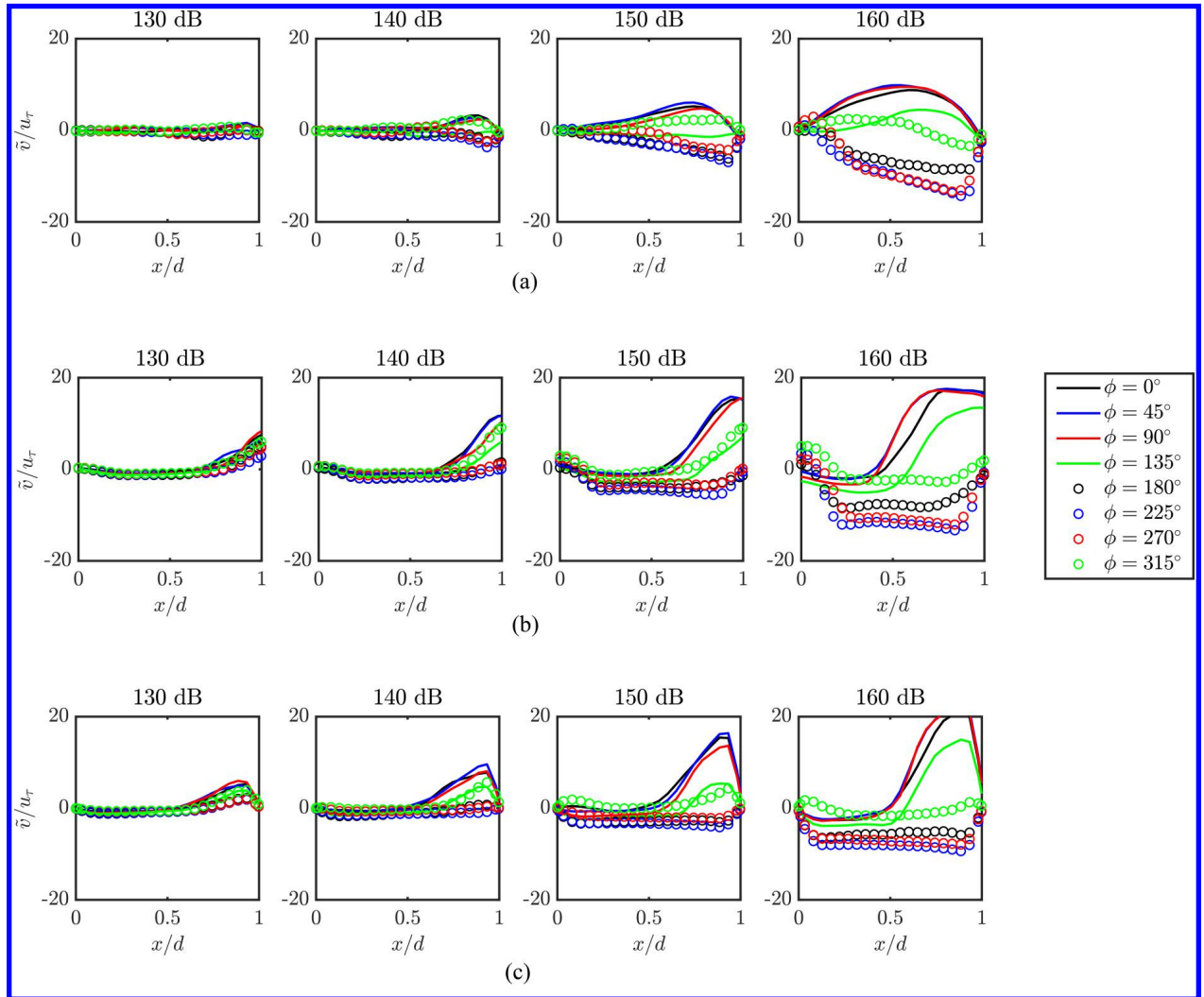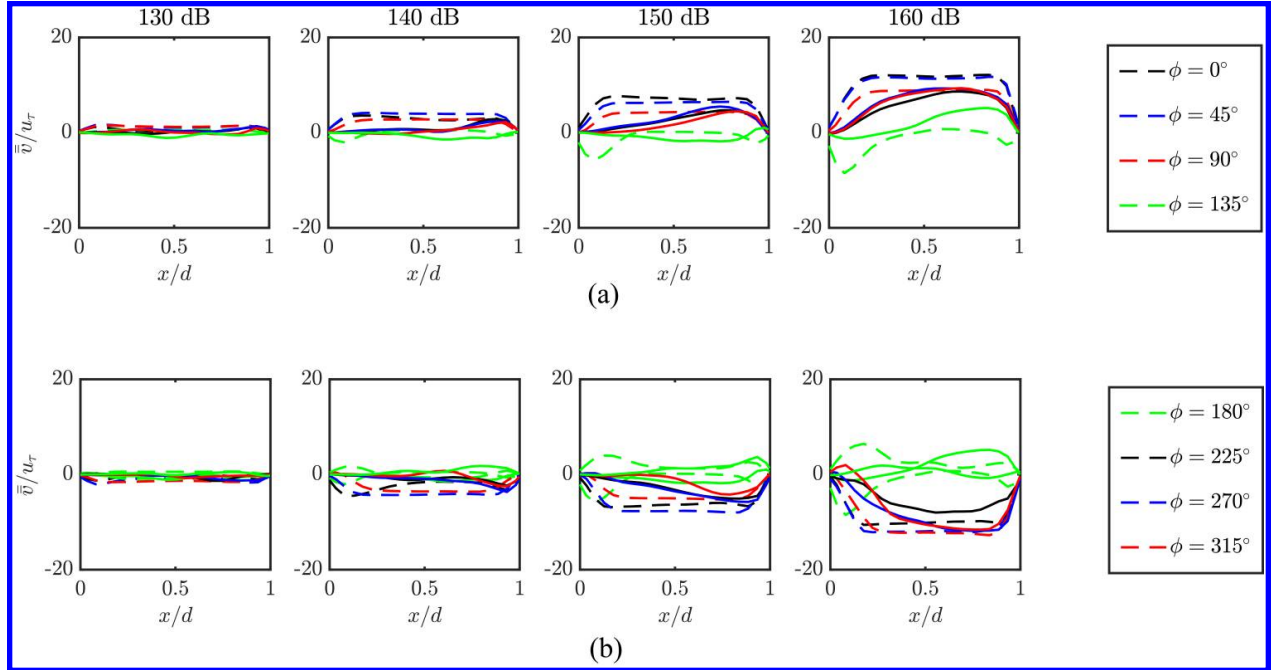
Fig. 7   Spatial distribution along the diameter of the phase-locked vertical velocity $\tilde{v}$ as a function of the SPL. (a) $y/\tau = 0$; (b) $y/\tau = 0.5$; (c) $y/\tau = 1$.
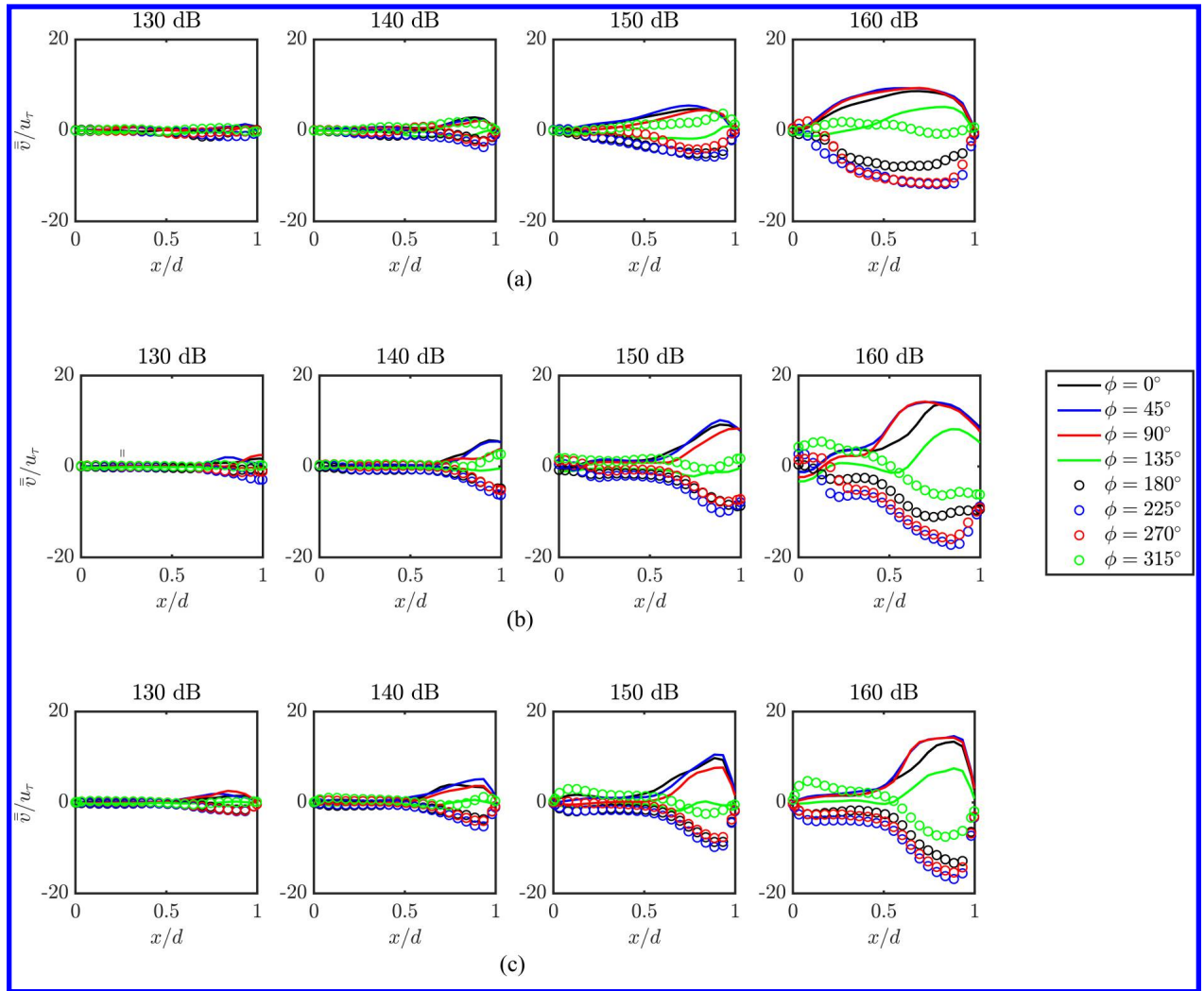
Fig. 8 Spatial distribution along the diameter of the acoustic-induced vertical velocity $\bar{\bar{v}}$ as a function of the SPL. (a) $y/\tau = 0$; (b) $y/\tau = 0.5$; (c) $y/\tau = 1$.

Fig. 9   Spatial distribution along the diameter of the acoustic-induced vertical velocity $\bar{\bar{v}}$ as a function of the SPL. Continuous line are for the case at M = 0.3, while dashed lines for the case at M = 0.   (a) Phase angle between $0° \leq \phi < 180°$ and (b) $180° \leq \phi < 360°$.

the figure are mainly due a difference in phase between the flow and no-flow cases. As a matter of fact, as described above, the phase equal to 0° is defined as the local maximum of the acoustic pressure outside of the boundary layer; as a consequence the effect of the shear within the boundary layer are not accounted for. This result suggests that the acoustic response of the liner, in terms of amplitude of $\bar{\bar{v}}$, to the grazing acoustic wave is almost unaffected by the presence of the grazing turbulent boundary layer if not for its spatial distribution that is altered by the mean flow.

These findings suggest that the increase in resistance is mainly due to the smaller cross-section of the orifice where a periodic variation of $\bar{\bar{v}}$ is found. However, the flow within the orifice is not symmetric in presence of turbulent grazing flow. For this reason, the mass-flow rate $\dot{m} = \rho \bar{\bar{v}} A$ at $y/\tau = 0.5$ is plotted for the flow and no-flow cases. Even if not plotted here, a similar behaviour has been found for $y/\tau = 0$ and 1. In the equation, A is the area of the orifice-cross section. For each SPL, it is evident that the shape of the curves is similar but the case with no-grazing flow has a larger $\dot{m}$ with respect to the grazing flow case. When increasing the SPL, in agreement with the previous observations, $\dot{m}$ becomes comparable for the two cases; however, the no-flow case shows more visible differences between the in-flow and out-flow phases, which are attributed to a fully non-linear behaviour of the liner [15]. The ratio of $\dot{m}$ for both cases is plotted in Figure 11 as a function of the SPL. Is it found that the ratio of $\dot{m}$ at $y/\tau = 0.5$ shows a trend and amplitude similar to the variation of θ as a function of frequency shown in Figure 2. This suggests that the effect of the mean flow within the orifice is an essential component to model and that it dominates the acoustic response of the liner.

VI. Conclusions

High-fidelity LB/VLES have been carried out to investigate the behaviour of a single-cavity multi-orifice acoustic liner grazed by a turbulent boundary layer at free-stream Mach number equal to 0.3 and an acoustic wave. Results from simulations with and without grazing acoustic wave have compared in order to analyze the acoustic-induced velocity within the orifice.

The acoustic-induced velocity within the liner orifice has been obtained through a triple decomposition approach: numerical results have been first phase-locked with respect to the grazing acoustic wave; then the acoustic-induced velocity is obtained as the phase-locked fields with its phase-average subtracted.

Results have shown that the acoustic-induced velocity shows a symmetric behaviour between the inflow and outflow cycles and that its amplitude is the same as for the case without turbulent grazing flow. The major differences when

10
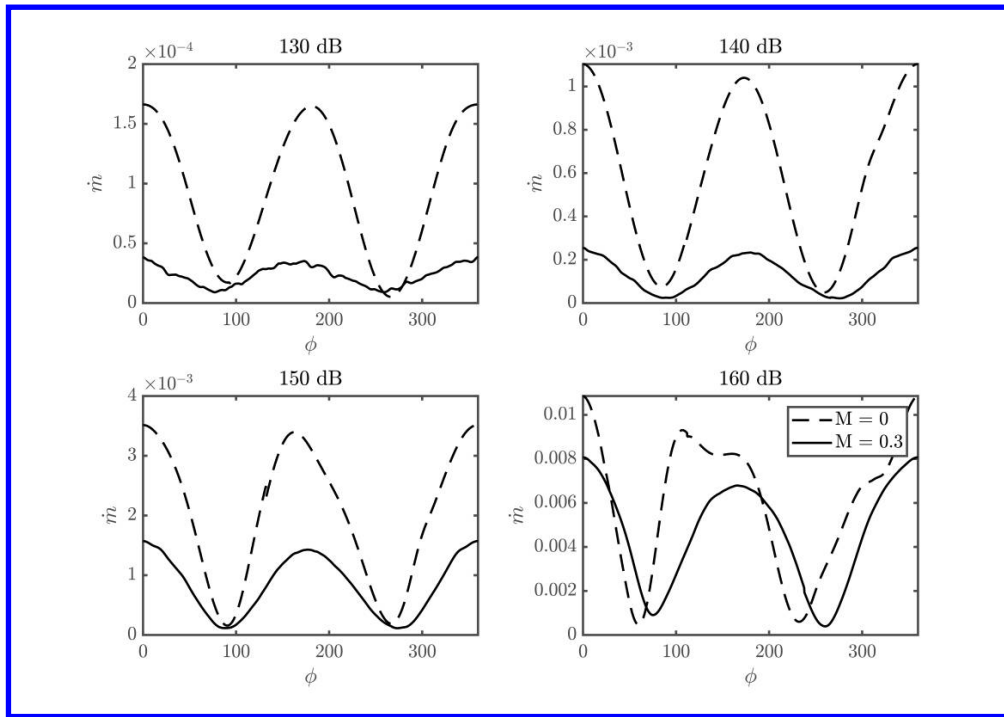
Fig. 10   Mass flow rate $\dot{m}$ as a function of the phase angle ϕ with and without grazing turbulent flow at different SPL.
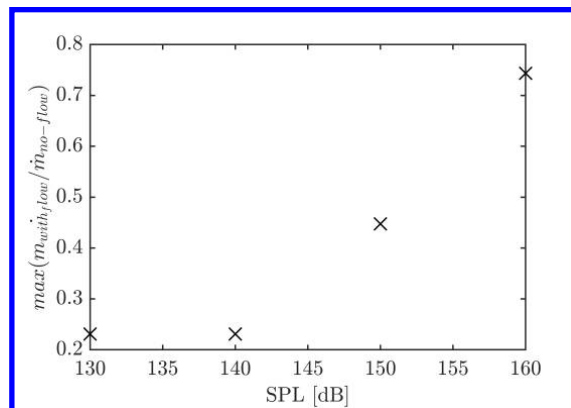
Fig. 11   Ratio between the mass flow rate $\dot{m}$ with and without grazing turbulent flow as a function of the phase angle ϕ at different SPL.

11

comparing the case with and without turbulent grazing flow is the spatial distribution within the orifice. The case with grazing turbulent flow shows an asymmetric distribution along the diameter with respect to the center of the orifice. This is caused by the effect of a quasi-steady vortex formed within the orifice; this vortex is localized in the upstream half of the orifice and allows the acoustic wave to penetrate within the orifice only where it shows the vertical velocity component oriented towards the cavity of the liner. This suggests that the differences in acoustic resistance is mainly caused by a reduction of the effective area of the orifice.

This has been confirmed by comparing the ratio of the mass-flow rate between the cases with and without grazing flow with the variation of resistance. It is shown that they are very similar in terms of both trends and amplitude.

Future work will be devoted to the analysis of the spatial dependence between the orifices and to the dependence to the free-stream Mach number.

Acknowledgments

References

[1] Aurégan, Y., "On the use of a Stress-Impedance Model to describe sound propagation in a lined duct with grazing flow," *Journal of Acoustic Socity of America*, Vol. 143, No. 5, 2018, pp. 2975–2979. https://doi.org/10.1121/1.5037585, URL https://doi.org/10.1121/1.5037585.

[2] Zhang, Q., and Bodony, D., "Numerical investigation of a honeycomb liner grazed by laminar and turbulent boundary layers," *Journal of Fluid Mechanics*, Vol. 792, 2016, pp. 936–980. https://doi.org/10.1017/jfm.2016.79.

[3] Myers, M. K., "On the acoustic boundary condition in the presence of flow," *Journal of Sound and Vibration*, Vol. 71, No. 3, 1980, pp. 429–434. https://doi.org/10.1016/0022-460X(80)90424-1.

[4] Khamis, D., and Brambley, E., "Acoustic boundary conditions at an impedance lining in inviscid shear flow," *Journal of Fluid Mechanics*, Vol. 796, 2016, pp. 386–416. https://doi.org/10.1017/jfm.2016.273, URL http://www.journals.cambridge.org/abstract_S0022112016002731.

[5] Ingard, U., "Influence of Fluid Motion Past a Plane Boundary on Sound Reflection, Absorption, and Transmission," *The Journal of the Acoustical Society of America*, Vol. 31, No. 7, 1959, pp. 1035–1036. https://doi.org/10.1121/1.1907805.

[6] Aurégan, Y., Starobinski, R., and Pagneux, V., "Influence of grazing flow and dissipation effects on the acoustic boundary conditions at a lined wall," *The Journal of the Acoustical Society of America*, Vol. 109, No. 1, 2001, pp. 59–64. https://doi.org/10.1121/1.1331678.

[7] Weng, C., Schulz, A., Ronneberger, D., Enghardt, L., and Bake, F., "Flow and Viscous Effects on Impedance Eduction," *AIAA Journal*, 2017, pp. 1–15. https://doi.org/10.2514/1.J055838.

[8] Schulz, A., Weng, C., Bake, F., Enghardt, L., and Ronneberger, D., "Modeling of liner impedance with grazing shear flow using a new momentum transfer boundary condition," *23rd AIAA/CEAS Aeroacoustics Conference*, American Institute of Aeronautics and Astronautics, Reston, Virginia, 2017, pp. 2017–3377. https://doi.org/10.2514/6.2017-3377, URL https://arc.aiaa.org/doi/10.2514/6.2017-3377.

[9] Renou, Y., and Aurégan, Y., "Failure of the Ingard–Myers boundary condition for a lined duct: An experimental investigation," *The Journal of the Acoustical Society of America*, Vol. 130, No. 1, 2011, pp. 52–60. https://doi.org/10.1121/1.3586789.

[10] Spillere, A., Bonomo, L., Cordioli, J., and Brambley, E., "Experimentally testing impedance boundary conditions for acoustic liners with flow: beyond upstream and downstream," *Journal of Sound and Vibration*, 2020, p. 115676. https://doi.org/10.1016/j.jsv.2020.115676.

[11] Jones, M., Watson, W., Parrott, T., and Smith, C., "Design and Evaluation of Modifications to the NASA Langley Flow Impedance Tube," *10th AIAA/CEAS Aeroacoustics Conference*, American Institute of Aeronautics and Astronautics, Reston, Virigina, 2004, pp. 2004–2837. https://doi.org/10.2514/6.2004-2837, URL http://arc.aiaa.org/doi/10.2514/6.2004-2837.

[12] Sebastian, R., Marx, D., Fortuné, V., and Lamballais, E., "Numerical simulation of a compressible channel flow with an acoustic liner," *23rd AIAA/CEAS Aeroacoustics Conference*, 2017, pp. 2017–4034. https://doi.org/10.2514/6.2017-4034, URL https://arc.aiaa.org/doi/pdf/10.2514/6.2017-4034.

[13] Mann, A., Perot, F., Kim, M.-S., and Casalino, D., "Characterization of Acoustic Liners Absorption using a Lattice-Boltzmann Method," *19th AIAA/CEAS Aeroacoustics Conference*, 2013, pp. 2013–2271. https://doi.org/10.2514/6.2013-2271, URL http://arc.aiaa.org/doi/10.2514/6.2013-2271.

[14] Hazir, A., and Casalino, D., "Effect of Temperature Variations on the Acoustic Properties of Engine Liners," *23rd AIAA/CEAS Aeroacoustics Conference*, 2017, pp. 2017–3874. https://doi.org/10.2514/6.2017-3874, URL https://arc.aiaa.org/doi/10.2514/6. 2017-3874.

[15] Manjunath, P., Avallone, F., Casalino, D., Ragni, D., and Snellen, M., "Characterization of Liners using a Lattice-Boltzmann Solver," *2018 AIAA/CEAS Aeroacoustics Conference*, 2018, pp. 2018–4192. https://doi.org/10.2514/6.2018-4192, URL https://arc.aiaa.org/doi/10.2514/6.2018-4192.

[16] Avallone, F., Manjunath, P., Ragni, D., and Casalino, D., "Lattice-Boltzmann Very Large Eddy Simulation of a Multi-Orifice Acoustic Liner with Turbulent Grazing Flow," *25th AIAA/CEAS Aeroacoustics Conference*, 2019, pp. 2019–2542. https://doi.org/10.2514/6.2019-2542, URL https://arc.aiaa.org/doi/10.2514/6.2019-2542.

[17] Casalino, D., Hazir, A., and Mann, A., "Turbofan Broadband Noise Prediction Using the Lattice Boltzmann Method," *AIAA Journal*, Vol. 56, No. 2, 2017, pp. 1–20. https://doi.org/10.2514/1.J055674, URL https://arc.aiaa.org/doi/10.2514/1.J055674.

[18] Shur, M., Strelets, M., Travin, A., Suzuki, T., and Spalart, P. R., "Unsteady Simulation of Sound Propagation in Turbulent Flow Inside a Lined Duct Using a Broadband Time-Domain Impedance Model," *AIAA AVIATION 2020 FORUM*, 2020, pp. 2020–2535. https://doi.org/10.2514/6.2020-2535, URL https://arc.aiaa.org/doi/10.2514/6.2020-2535.

[19] Shan, X., Yuan, X.-F., and Chen, H., "Kinetic theory representation of hydrodynamics: a way beyond the Navier–Stokes equation," *Journal of Fluid Mechanics*, Vol. 550, 2006, pp. 413–441. https://doi.org/10.1017/S0022112005008153.

[20] Chen, H., Orszag, S., Staroselsky, I., and Succi, S., "Expanded analogy between Boltzmann kinetic theory of fluids and turbulence," *Journal of Fluid Mechanics*, Vol. 519, 2004, pp. 301–314. https://doi.org/10.1017/S0022112004001211, URL https://doi.org/10.1017/S0022112004001211.

[21] Yakhot, V., Orszag, S., Thangam, S., Gatski, T., and Speziale, C., "Development of turbulence models for shear flows by a double expansion technique," *Physics of Fluids A*, Vol. 4, No. 7, 1992, pp. 1510–1520. https://doi.org/10.1063/1.858424, URL http://aip.scitation.org/doi/10.1063/1.858424.

[22] Teixeira, C., "Incorporating Turbulence Models into the Lattice-Boltzmann Method," *International Journal of Modern Physics C*, Vol. 09, No. 08, 1998, pp. 1159–1175. https://doi.org/10.1142/S0129183198001060.

[23] Jones, M., Watson, W., and Nark, D., "Effects of Flow Profile on Educed Acoustic Liner Impedance," *16th AIAA/CEAS Aeroacoustics Conference*, 2010, pp. 2010–3763. https://doi.org/10.2514/6.2010-3763.

[24] Dean, P., "An in situ method of wall acoustic impedance measurement in flow ducts," *Journal of Sound and Vibration*, Vol. 34, No. 1, 1974, pp. 97–IN6. https://doi.org/10.1016/S0022-460X(74)80357-3.

[25] Léon, O., Méry, F., Piot, E., and Conte, C., "Near-wall aerodynamic response of an acoustic liner to harmonic excitation with grazing flow," *Experiments in Fluids*, Vol. 60, No. 9, 2019, pp. 1–18. https://doi.org/10.1007/s00348-019-2791-5.